The neutron capture cross section of ^{232}Th measured at the n_TOF facility at CERN in the unresolved resonance region up to 1 MeV

G. Aerts,[1] U. Abbondanno,[2] H. Álvarez,[3] F. Alvarez-Velarde,[4] S. Andriamonje,[1] J. Andrzejewski,[5] P. Assimakopoulos,[6] L. Audouin,[7] G. Badurek,[8] P. Baumann,[9] F. Bečvář,[10] E. Berthoumieux,[1] F. Calviño,[11] D. Cano-Ott,[4] R. Capote,[12,13] A. Carrillo de Albornoz,[14] P. Cennini,[15] V. Chepel,[16] E. Chiaveri,[15] N. Colonna,[17] G. Cortes,[11] A. Couture,[18] J. Cox,[18] M. Dahlfors,[15] S. David,[9] I. Dillman,[7] R. Dolfini,[19] C. Domingo-Pardo,[20] W. Dridi,[1] I. Duran,[3] C. Eleftheriadis,[21] M. Embid-Segura,[4] L. Ferrant,[22] A. Ferrari,[15] R. Ferreira-Marques,[16] L. Fitzpatrick,[15] H. Frais-Koelbl,[23] K. Fujii,[2] W. Furman,[24] I. Goncalves,[16] E. Gonzalez-Romero,[4] A. Goverdovski,[25] F. Gramegna,[26] E. Griesmayer,[23] C. Guerrero,[4] F. Gunsing,[1,*] B. Haas,[27] R. Haight,[28] M. Heil,[7] A. Herrera-Martinez,[15] M. Igashira,[29] S. Isaev,[22] E. Jericha,[8] F. Käppeler,[7] Y. Kadi,[15] D. Karadimos,[6] D. Karamanis,[6] M. Kerveno,[9] V. Ketlerov,[25,15] P. Koehler,[30] V. Konovalov,[24,15] E. Kossionides,[31] M. Krtička,[10] C. Lamboudis,[21] H. Leeb,[8] A. Lindote,[16] I. Lopes,[16] M. Lozano,[13] S. Lukic,[9] J. Marganiec,[5] L. Marques,[14] S. Marrone,[17] P. Mastinu,[26] A. Mengoni,[23,15] P.M. Milazzo,[2] C. Moreau,[2] M. Mosconi,[7] F. Neves,[16] H. Oberhummer,[8] S. O'Brien,[18] M. Oshima,[32] J. Pancin,[1] C. Papachristodoulou,[6] C. Papadopoulos,[33] C. Paradela,[3] N. Patronis,[6] A. Pavlik,[34] P. Pavlopoulos,[35] L. Perrot,[1] M.T. Pigni,[8] R. Plag,[7] A. Plompen,[36] A. Plukis,[1] A. Poch,[11] C. Pretel,[11] J. Quesada,[13] T. Rauscher,[37] R. Reifarth,[28] M. Rosetti,[38] C. Rubbia,[19] G. Rudolf,[9] P. Rullhusen,[36] J. Salgado,[14] L. Sarchiapone,[15] I. Savvidis,[21] C. Stephan,[22] G. Tagliente,[17] J.L. Tain,[20] L. Tassan-Got,[22] L. Tavora,[14] R. Terlizzi,[17] G. Vannini,[39] P. Vaz,[14] A. Ventura,[38] D. Villamarin,[4] M.C. Vincente,[4] V. Vlachoudis,[15] R. Vlastou,[33] F. Voss,[7] S. Walter,[7] H. Wendler,[15] M. Wiescher,[18] and K. Wisshak[7]

(The n_TOF Collaboration)

[1] *CEA/Saclay - DSM/DAPNIA, Gif-sur-Yvette, France*
[2] *Istituto Nazionale di Fisica Nucleare, Trieste, Italy*
[3] *Universidade de Santiago de Compostela, Spain*
[4] *Centro de Investigaciones Energeticas Medioambientales y Technologicas, Madrid, Spain*
[5] *University of Lodz, Lodz, Poland*
[6] *University of Ioannina, Greece*
[7] *Forschungszentrum Karlsruhe GmbH (FZK), Institut für Kernphysik, Germany*
[8] *Atominstitut der Österreichischen Universitäten,Technische Universität Wien, Austria*
[9] *Centre National de la Recherche Scientifique/IN2P3 - IReS, Strasbourg, France*
[10] *Charles University, Prague, Czech Republic*
[11] *Universitat Politecnica de Catalunya, Barcelona, Spain*
[12] *International Atomic Energy Agency, NAPC/Nuclear Data Section, Vienna, Austria*
[13] *Universidad de Sevilla, Spain*
[14] *Instituto Tecnológico e Nuclear(ITN), Lisbon, Portugal*
[15] *CERN, Geneva, Switzerland*
[16] *LIP - Coimbra & Departamento de Fisica da Universidade de Coimbra, Portugal*
[17] *Istituto Nazionale di Fisica Nucleare, Bari, Italy*
[18] *University of Notre Dame, Notre Dame, USA*
[19] *Università degli Studi Pavia, Pavia, Italy*
[20] *Instituto de Física Corpuscular, CSIC-Universidad de Valencia, Spain*
[21] *Aristotle University of Thessaloniki, Greece*
[22] *Centre National de la Recherche Scientifique/IN2P3 - IPN, Orsay, France*
[23] *International Atomic Energy Agency (IAEA), Nuclear Data Section, Vienna, Austria*
[24] *Joint Institute for Nuclear Research, Frank Laboratory of Neutron Physics, Dubna, Russia*
[25] *Institute of Physics and Power Engineering, Kaluga region, Obninsk, Russia*
[26] *Istituto Nazionale di Fisica Nucleare(INFN), Laboratori Nazionali di Legnaro, Italy*
[27] *Centre National de la Recherche Scientifique/IN2P3 - CENBG, Bordeaux, France*
[28] *Los Alamos National Laboratory, New Mexico, USA*
[29] *Tokyo Institute of Technology, Tokyo, Japan*
[30] *Oak Ridge National Laboratory, Physics Division, Oak Ridge, USA*
[31] *NCSR, Athens, Greece*
[32] *Japan Atomic Energy Research Institute, Tokai-mura, Japan*
[33] *National Technical University of Athens, Greece*
[34] *Institut für Isotopenforschung und Kernphysik, Universität Wien, Austria*
[35] *Pôle Universitaire Léonard de Vinci, Paris La Défense, France*
[36] *CEC-JRC-IRMM, Geel, Belgium*
[37] *Department of Physics and Astronomy - University of Basel, Basel, Switzerland*
[38] *ENEA, Bologna, Italy*

[39]*Dipartimento di Fisica, Università di Bologna, and Sezione INFN di Bologna, Italy*
(Dated: April 11, 2006)

We have measured the neutron capture reaction yield of ^{232}Th at the neutron time-of-flight facility n_TOF at CERN in the energy range from 1 eV to 1 MeV. The average capture cross section has been extracted in the energy range from 4 keV up to 1 MeV with an overall accuracy better than 4%. An independent IAEA evaluation shows good agreement with the data. The average cross section has been expressed in terms of average resonance parameters using the partial waves $\ell = 0, 1$, and 2.

PACS numbers: 25.40.Lw, 25.40.Ny, 28.20.Fc

I. INTRODUCTION

Accurate knowledge of neutron-nucleus reaction cross sections is of primary importance for studies of stellar nucleosynthesis [1, 2], fundamental symmetries, [3, 4] and applications of nuclear technology [5–8]. In addition, important information on level densities, a key ingredient in many nuclear structure and reaction models, can be obtained directly from high resolution neutron resonance spectroscopy. Research activities related to for example neutron capture stellar nucleosynthesis, neutron-induced symmetry breaking reactions, but also to applications like the transmutation of nuclear waste, accelerator driven systems (ADS) and the thorium-based nuclear fuel cycle, have pointed out that for many nuclides the available experimental information is of insufficient accuracy or sometimes lacking. Neutron cross section data are available by means of compilations of experimental data [9, 10] or through evaluated nuclear data libraries such as BROND, ENDF, JEFF, and JENDL[11]. The necessary update of these neutron cross section libraries rely on the availability of accurate measurements obtainable at advanced neutron sources.

The low-energy p-wave resonances in ^{232}Th have received little attention since they do not contribute significantly to multigroup cross sections. However, large parity-nonconservation effects have been observed in p-wave resonances of several isotopes, measured by the asymmetry of the neutron transmission of polarized neutrons on unpolarized nuclei [3, 12]. These effects, in the order of 10^{-7} in nucleon-nucleon interactions, were found to be up to 10% for ^{232}Th in transmission experiments. [13, 14]. A more precise knowledge of the p-wave neutron widths Γ_n may improve the extraction of the parity-nonconserving matrix elements.

The use of thorium in the nuclear fuel cycle for either critical or subcritical systems is nowadays a topic of great interest. This cycle is based on the fertile ^{232}Th and the fissile ^{233}U, formed by the neutron capture on ^{232}Th and the subsequent beta decays of ^{233}Th and ^{233}Pa. An interesting advantage in using this fuel cycle, as compared to the conventional uranium/plutonium cycle, which is currently used in all operating power plants, is related to its low production of high-mass actinides. In the uranium cycle the fuel contains a large fraction of $^{238}_{92}$U, which is the seed for the production of higher actinides by successive neutron captures and fast beta decays. The use of the lighter nucleus $^{232}_{90}$Th reduces significantly the radiotoxicity of the spent fuel by a much lower build-up of heavy trans-uranium isotopes, in particular plutonium, americium and curium.

The cross section of the ^{232}Th neutron capture reaction is a crucial input parameter for the design of any nuclear system based on the thorium fuel cycle. The presently available nuclear data libraries for the ^{232}Th(n,γ) cross section are mainly based on less recent and discrepant experiments [15–23]. This situation prompted the new neutron capture experiments carried on recently. Most of them have been performed using the neutron time-of-flight technique. Baek *et al.* [24] investigated the gamma-ray multiplicity and the capture cross section in the energy region between 21.5 and 215 eV. Grigoriev *et al.* [25] measured the average cross section in the energy region between 10 eV and 10 keV. In the unresolved resonance region, Borella *et al.* [26] have measured the cross section between 5 and 150 keV. The measurement of Wisshak *et al.* [27] covered the region between 5 and 225 keV. Finally, Karamanis *et al.* [28] used the activation technique to measure the capture cross section between 60 keV and 2 MeV. Although considerable improvements could be achieved, the discrepancies in the ^{232}Th(n,γ) cross section below the fission threshold, i.e. in the important energy range below 1 MeV, could not be removed.

In order to study neutron induced reactions for nuclear technology, nuclear astrophysics, and nuclear structure and reaction physics, a new neutron time-of-flight facility, n_TOF, has been recently constructed at CERN, Geneva. This facility has a very high instantaneous neutron flux, which results in a favorable signal to noise ratio for neutron capture experiments of radioactive isotopes. This is a major advantage for a measurement of the ^{232}Th(n,γ) cross section. In fact, the high energy gamma rays going up to 2.6 MeV, originating from the beta decay of the daughter product ^{208}Tl, were severely hindering the accuracy of previous capture measurements. This component of the background is strongly reduced in the n_TOF setup. The second advantage of the n_TOF facility is the low duty cycle with a large spacing in time between consecutive time-of-flight bursts, allowing to measure a wide energy range in a single experiment.

*corresponding author: F. Gunsing, gunsing@cea.fr

We have measured in a single experiment the neutron capture cross section of ^{232}Th in the neutron energy range from 1 eV to 1 MeV. The analysis procedure and the type of results for the resolved and unresolved resonance region is very different. Therefore the resolved resonance part will be described separately in a later paper [29]. In this paper we give the average cross section in the unresolved resonance region from 4 keV up to 1 MeV. No other measurement has covered this wide energy range in a single experiment. This work has been part of a PhD thesis [30].

II. EXPERIMENTAL DETAILS

A. The n_TOF beam and the capture setup

The n_TOF facility, based on an idea by Rubbia *et al.* [31], became fully operational in May 2002, when the scientific program started. A detailed description of its performances can be found elsewhere [32]. Here we will mention the basic characteristics of the facility. At n_TOF, neutrons are produced by spallation reactions induced by a pulsed, 6 ns wide, 20 GeV/c proton beam with up to 7×10^{12} protons per pulse, impinging on a 80x80x60 cm^3 lead target. A 5 cm water slab surrounding the lead target serves as a coolant and at the same time as a moderator of the initially fast neutron spectrum, providing a wide energy spectrum from 1 eV to about 250 MeV with a nearly $1/E$ isolethargic flux dependence up to 1 MeV. An evacuated neutron beam line leads to the experimental area with the capture sample position at 185.2 m from the lead target.

Two collimators are present in the neutron beam, one with a diameter of 13.5 cm placed at 135 m from the lead target and one at 175 m with a diameter of 2 cm for the capture measurements. This collimation results in a nearly symmetric Gaussian-shaped beam profile at the sample position, with an energy dependent standard deviation, which is about 0.77 cm at low neutron energies [33].

At a distance of 145 m a 1.5 T magnet is placed in order to remove the residual charged particles going along the neutron beam line. A previously observed background due to negative muon capture has been drastically reduced by means of a 3 m thick iron shielding located after the sweeping magnet [34, 35]. The neutron beam line extends for an additional 12 m beyond the experimental area to minimize the background from back-scattered neutrons. The repetition period of the proton pulses of 2.4 seconds on average is low enough to prevent any overlapping of neutrons in subsequent cycles.

At the sample position located at a flight length of 185.2 m, two disc-shaped thorium samples with a diameter of 1.5 cm and with a total mass of 2.8037 g and a purity of 99.5% were put together and placed inside a remotely controlled carbon fibre vacuum sample changer. With this sample thickness some low-energy resonances

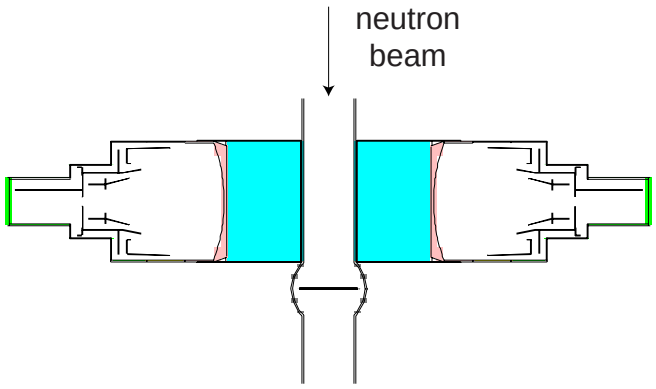

FIG. 1: (Color online) A schematic view of the horizontal plane of the detectors and sample geometry in the ^{232}Th(n,γ) measurement. Neutrons going through the 5.8 cm inner diameter beam tube are incident on the sample placed in the beam. Two C_6D_6 detectors, each one consisting of a scintillator cell of 12.7 cm in diameter and 7.62 cm high coupled to a photomultiplier, are placed 9.2 cm upstream with respect to the sample center.

are saturated allowing to obtain an absolute normalization of the capture yields. The samples were mounted on thin kapton foils stretched over a carbon fibre frame that was much larger than the neutron beam, thus avoiding neutron scattering from the support. In addition to the thorium samples, we have measured under the same conditions also samples of gold (1.33 g) to verify the analysis procedure, and of natural lead (2.04 g) to estimate the background due to in-beam photons scattered from the sample. All samples were 15 mm in diameter. The scattered photon spectrum arose mainly from 2.23 MeV gamma rays from neutron capture on hydrogen in the water moderator and coolant surrounding the neutron spallation target.

The sample was viewed by two in-house developed gamma-ray detectors [36], each one consisting of about 1 liter of C_6D_6 liquid scintillator contained in a cylindrical low mass carbon fibre housing, 12.7 cm in diameter and 7.62 cm high. Both carbon and deuterium have a very low neutron capture cross section and therefore do not significantly contribute to the background from sample-scattered neutron capture in the detector material. The scintillator was coupled directly, without an intermediate quartz window usually present in this type of detector, to an EMI-9823QKB photomultiplier tube. The detectors were placed perpendicular to the beam, 9.2 cm upstream from the sample center in order to reduce the background due to scattered photons. This geometrical configuration also allows to reduce the effects of the angular distribution from primary neutron capture gamma rays following neutron capture in $\ell = 1$ p-wave resonances with spin 3/2. The setup of the sample-detector geometry is sketched in figure 1. An in-beam neutron flux monitor [37], consisting of a ^{6}Li deposit on a mylar foil and 4 off-beam silicon detectors measuring the particles from the

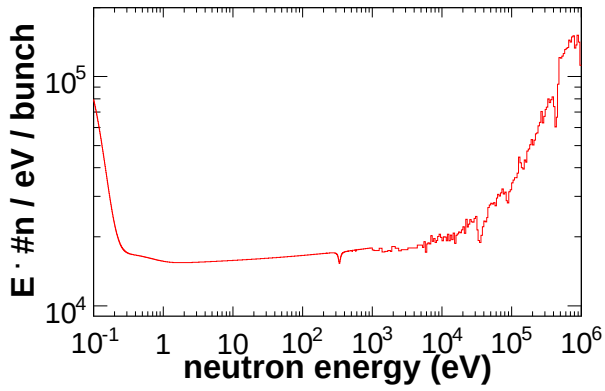

FIG. 2: (Color online) The energy density, multiplied by the kinetic energy, of the total number of neutrons $\#n$ incident on the sample plane for a standard burst of 7×10^{12} protons as a function of the neutron energy. The energy density is given in units $dn/d\ln(E) = E \cdot dn/dE$.

^{6}Li(n,α)T reaction, was located about 3 m upstream of the sample position.

The energy density of the number of neutrons crossing the plane perpendicular to the beam at the sample position at 185.2 m for a standard burst of 7×10^{12} protons of 20 GeV/c, is shown in figure 2 as a function of neutron energy. This quantity will be called neutron flux in the following. The neutron flux is given in isolethargic units $d\Phi(E)/d\ln E$. These data are based on a measurement performed with a ^{235}U loaded parallel plate fission ionization chamber from the Physikalisch-Technische Bundesanstalt in Braunschweig [38]. The raw counting spectra resulting from this flux measurement have statistical uncertainties between 1 and 1.8% per bin (20 bins per decade) in the neutron energy range from 1 keV to 1 MeV. At neutron energies below 1 keV, we used the data from the ^{6}Li-based in-beam neutron flux monitor [37], with much lower statistical uncertainties. In our analysis of the ^{232}Th cross section measurement, the absolute normalization of the capture yields is obtained independently from a low-energy saturated resonance. Therefore, the absolute value of the flux is not necessary but only its relative energy dependence from approximately 1 eV up to 1 MeV is used in the analysis. We estimate this value to be 2% at maximum based on the matching of the flux obtained from the ^{6}Li neutron monitor and the ^{235}U fission chamber around 1 keV. The electric signals from the photomultipliers of the detectors were sampled with a frequency of 0.5 GHz, during 16 ms after each proton pulse, with 8 bit resolution using an Acqiris Cougar 2010-4 flash ADC. The raw data for each pulse were transferred to the CERN's central data recording system for off-line analysis. The pulse repetition interval was at minimum 1.2 s. For each event the pulse height, proportional to the deposited energy in the C_6D_6 detector, and the neutron time-of-flight were extracted from the recorded signals. An effective threshold of 160 keV detected energy resulted from the pulse extraction for this case. More details on the data acquisition system can be found in reference [39].

The use of flash ADCs for the data acquisition reduces the dead time to an effective value of about 25 nanoseconds, related to the software for pulse extraction. The effect does not exceed 2% below 500 keV, except for large local count rates as in the peaks of large resonances. In the off-line event processing we applied a fixed dead time of 30 ns, for which the count rate was corrected. When an event was observed in one of the two detectors, all events occurring within 30 ns in both detectors were discarded in order to eliminate coincidence counting.

B. Determination of the capture yield

The capture yield $Y(E_n)$, which is the fraction of the number of incident neutrons $\Phi(E_n)$ with energy E_n incident on the sample that leads to a capture event, cannot be determined in a straightforward way from the observed time-of-flight spectra $C_{\rm obs}(E_n)$. In fact, without considering background, this is given by

$$C_{\rm obs}(E_n) = \Phi(E_n) Y(E_n) \epsilon_c \qquad (1)$$

where the efficiency ϵ_c for detecting the capture event depends in a complex way on the emitted gamma-ray spectrum when using a low efficiency detector like the C_6D_6 detectors of this experiment. The gamma-ray spectrum is different for each isotope and for a given isotope differs from one resonance to another. The neutron capture event is characterized by the de-excitation of the the compound nucleus by emission of one or more gamma rays. A calculation with a simulation code [40] indicates that the multiplicity of the ^{233}Th compound decay is ≈ 3 and goes through a cascade onto the several tens of thousands of available levels, like most medium and heavy mass nuclei. To circumvent this problem it is preferable to have the detector efficiency proportional to the gamma-ray energy E_γ and a detection efficiency low enough to detect at most one gamma ray of the cascade. In that case the efficiency for the cascade can be shown to be proportional to the total gamma energy released in the capture event $\epsilon_c = kE_c$ with proportionality k, and it is therefore independent from the details of the gamma decay path. The gamma-ray efficiency is related to the detector response function r_γ by $\epsilon_\gamma = \int r_\gamma(E_d) dE_d$. The energy deposited in the detector E_d is in general not proportional to E_γ but this can be introduced artificially by modifying the response function using a weighting function $W(E_d)$ such that

$$\epsilon_\gamma = \int W(E_d) r_\gamma(E_d) dE_d = kE_\gamma \,. \qquad (2)$$

This method, known as the pulse height weighting technique (PHWT), is described extensively elsewhere

[41–43]. The weighting function can be accurately derived using Monte Carlo simulations of the detector response to different mono-energetic gamma rays. In the measurement, the detector response function to the neutron capture gamma-ray cascade $r_\gamma(E_d)$ is estimated by the measured count rate spectrum $R(E_d)$. Therefore the weighted count rate spectrum can be written as

$$C_{\rm W}(E_n) = \int R_\gamma(E_d) W(E_d) dE_d = \Phi(E_n) Y(E_n) E_c \quad (3)$$

taking the proportionality constant equal to 1 in inverse units of energy. After correction for background, the capture yield can be determined from the weighted count rate spectrum.

The pulse height distribution of the C_6D_6 detectors were calibrated regularly during the experiment using the radioactive sources ^{137}Cs, ^{60}Co and a composite source of the alpha-emitter ^{238}Pu and carbon, giving a 6.13 MeV gamma-ray through the ^{13}C(α, n)^{16}O* reaction.

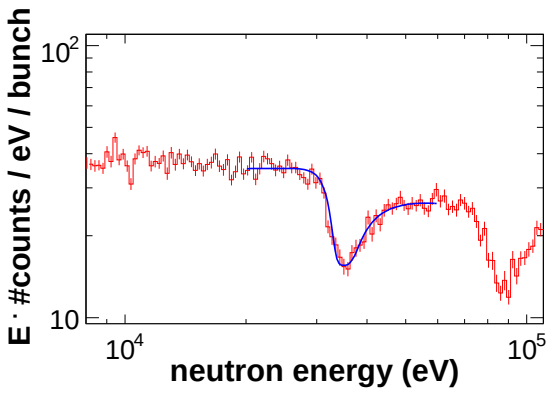

FIG. 3: (Color online) Part of the counting spectrum of the Th sample with the Al filter in the neutron beam together with the fit of the 34.8 keV black resonance of Al. The energy density of the number of counts is given in units $1/d\ln(E) = E/dE$.

C. Determination of the background

Several components contribute to the background level in our capture measurement. A time independent background comes mainly from the radioactivity of the sample and has been measured with the neutron beam switched off. With the high instantaneous flux of the n_TOF installation this background is relevant only at low neutron energies and can be easily subtracted or fitted with the data.

The main source of background in the keV region of neutron energies is generated by the gamma rays present in the beam, which are scattered from the sample and detected in the C_6D_6 detectors. The majority of these gamma rays originated from neutron captures on hydrogen in the water moderator, but other gamma-ray components are present with relative intensities that vary slightly with time-of-flight. In order to quantitatively measure this background component we have performed a series of measurements with a 30 mm thick aluminum neutron black-resonance filter. These filters remove the neutrons from the beam at specific energies, corresponding to large resonances with zero transmission. The level of the background in a measurement with a black-resonance filter corresponds then to level of the valleys in the count rate at the filter resonance energies.

The neutron filter also attenuates the in-beam photons that are scattered from the sample. In order to obtain the background level in the measurement without filters, we have corrected for the attenuation of the in-beam gamma-rays by the filters. This is done by assuming that the shape of the scattered photon background $B_\gamma(t)$ as a function of time of flight t is independent of the sample, an assumption that we have confirmed by Monte Carlo simulations for the present cases. The shape of this background component has been determined by measuring, under the same conditions, a sample of natural lead. The ^{nat}Pb(n,γ) capture cross section is very low and the reaction rate in the keV neutron energy region is almost entirely due to in-beam sample scattered photons.

Measurements of a lead sample have been taken with and without the filters in the beam. After subtraction of the expected capture yield, which is small compared to the background, we obtained the background for the lead samples. The shape of the background for the lead sample without filters $B_{\rm Pb}$ is given by the two exponentials in brackets in eq. (4). From the ratio of the background spectra obtained for the lead sample with ($B_{\rm PbAl}$) and without ($B_{\rm Pb}$) filters, we determined the attenuation of the gamma rays $k_2(E_n) = B_{\rm PbAl}/B_{\rm Pb}$. The energy dependence of k_2 reflects the fact that the relative intensities of the in-beam gamma rays change with time-of-flight.

For the black resonance of Al at 34.8 keV all neutrons are removed from the beam and the remaining part is the background. A clear dip is visible in the spectrum. We determined the level of the dip due to the black resonance in the spectrum of thorium with the Al filter by fitting the expected shape of the resonance as a perturbation on a smooth reaction yield. The expected shape was calculated as a transmission using the total cross section of Al without the potential scattering contribution. In figure 3 the spectrum $B_{\rm ThAl}$ of the Th sample with the Al filter in the beam in the vicinity of the 34.8 keV resonance of Al is shown together with the fit. From the ratio $k_1 = B_{\rm ThAl}(34.8)/B_{\rm Pb}(34.8)$ of this level and the level of the background of lead without a filter we determined the background for the sample of thorium without filter. The uncertainty for the normalization of this background component, obtained from the fit and the variation from different binnings, is 2.5%.

At lower energies a time-of-flight dependent background could be determined in good approximation in between the resonances where the capture yield is very

low compared to the background. A small residual background will be fitted together with the resonance shapes. The total background obtained in this way, in counts per unit time-of-flight, could be parametrized as a function of the neutron time of flight t by

$$B(t) = a_1 t^{b_1} + \frac{k_1}{k_2(t)} \left[a_2 \exp(b_2 \cdot t) + a_3 \exp(b_3 \cdot t)\right] \quad (4)$$

where the first term corresponds to the low energy background and the exponents represent the photon induced background, with a_i and b_i suitably determined constants and with k_1 and $k_2(E_n)$ scaling factors explained in the text.

While our range of interest is below 1 MeV and is therefore below the fission threshold for ^{232}Th, contributions from the inelastic scattering channels, which are present from the first excited state of ^{232}Th at 49.4 keV, are a supplementary source of background. Although the detected energy of the gamma decay of this state and even of the next state is below the signal threshold of 160 keV, states with spins and parities allowing inelastic scattering become an important source of background from about 700 keV. Indeed the gamma rays from fission or inelastic scattering cannot be distinguished from the gamma rays from neutron capture with C_6D_6 detectors.

In order to exclude these background gamma rays we have repeated the analysis procedure applying a gamma-ray threshold of 1 MeV. This removes the background contributions from the (n,n'γ) reaction channels up to a neutron energy of 1 MeV at the expense of a reduction of the counting statistics. The count rate spectra and the backgrounds are shown in figure 4 for the two thresholds of 160 and 1000 keV.

Setting such a high threshold as 1 MeV may put the validity of the weighting function technique into question. However, the derived capture yields obtained using a threshold of 160 keV and of 1 MeV, and after normalization at the low-energy saturated resonances, turned out to be essentially identical within their error bars up to about 700 keV. As shown in figure 5 above 700 keV the gamma rays from inelastic scattering start to contribute to the background if a low threshold of 160 keV is applied, while this background is absent with the high threshold of 1 MeV. We explain this by the fact that the average gamma decay spectra for the thorium resonances are very similar because of the high level density and therefore the high number of states available for the gamma decay cascade. Since the measurement is self-normalized and hence not dependent on a reference measurement, any effect of a high gamma-ray threshold propagates in the same manner to the entire energy range. It is clear that this method of eliminating gamma rays from inelastically scattered neutrons may not be as straightforward when a reference measurement with a different isotope is used.

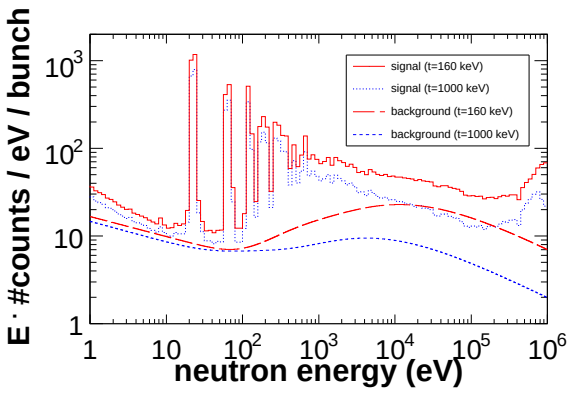

FIG. 4: (Color online) The measured count rate of the ^{232}Th(n,γ) reaction per bunch of 7×10^{12} protons and the derived background applying a gamma-ray threshold threshold of 160 and 1000 keV, respectively.

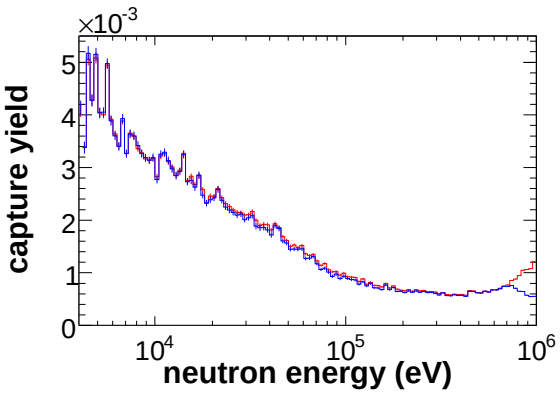

FIG. 5: (Color online) Derived capture yields using spectra with a gamma-ray threshold of 160 and 1000 keV respectively. Both yields are identical within their uncertainties up to a neutron energy of about 700 keV. Beyond that energy gamma rays from inelastic scattering become visible as a background that can be eliminated only with the high threshold.

III. RESULTS IN THE UNRESOLVED RESONANCE REGION

A. The capture cross section derived from the capture yield

The capture reaction yield as a function of neutron energy E_n is related to the capture cross section σ_γ and the total cross section σ_T by

$$Y(E_n) = \mu(E_n) \left(1 - e^{-n\sigma_T(E_n)}\right) \cdot \frac{\sigma_\gamma(E_n)}{\sigma_T(E_n)} \quad (5)$$

where $\mu(E_n)$ is the energy dependent multiple scattering correction. In the resolved resonance region the cross section is described by individual resonance parameters by means of the R-matrix formalism. In the unresolved res-

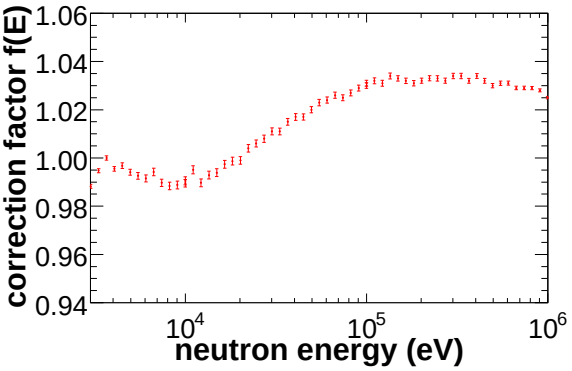

FIG. 6: (Color online) The correction factor $f(E_n)$ due to self absorption and multiple scattering calculated with the code SESH [44].

onance region resonances are overlapping and one measures an average capture yield $<Y(E_n)>$, which can be related to the average capture cross section by

$$<Y(E_n)>= f(E_n) \times n \times <\sigma_\gamma(E_n)> \qquad (6)$$

where n is the sample thickness in atoms per barn and $f(E_n)$ is the correction that accounts for self absorption and multiple scattering effects. This correction is in general not analytically determineable but can be obtained by Monte Carlo simulations. We have used the code SESH [44] to calculate this correction factor $f(E_n)$. This code calculates the correction by generating individual resonances according to user supplied level densities and neutron strength functions. The result of these calculations are shown in figure 6. The energy averaged cross section obtained in this way is reported in table I. In figure 7 the cross section is plotted, multiplied by $\sqrt{E_n}$ in order to appreciate the data in the entire energy range.

B. Comparison with existing data

The present measurement, covering the full energy range from 4 keV to 1 MeV, well above the inelastic scattering threshold, can be compared to existing measurements in the overlapping energy regions. The prompt gamma-ray data from Borella *et al.* [26] and the activation data from Lindner *et al.* [16] agree with the present results within the stated uncertainties. Also the data of Poenitz and Smith [18] correspond reasonably well. The activation data from Karamanis *et al.* [28] show the same the shape but are systematically lower than the present results in the overlapping energy range. The prompt gamma-ray data from Wisshak *et al.* [27] are discrepantly higher up to about 40% below 10 keV and slightly lower around 100 keV. Macklin *et al.* [45] and Kobayashi *et al.* [19] have used freshly isotopically separated ^{232}Th samples, reducing largely the background due to the radioactivity of the daughter nuclei

TABLE I: The measured capture cross section of the ^{232}Th(n,γ) reaction averaged over the neutron energy intervals $E_{\rm low}$ - $E_{\rm high}$. The quoted uncertainties are statistical uncertainties only. An overall uncertainty of 3.5% should be applied to the cross section values in the entire neutron energy range (see text for a detailed discussion).

$E_{\rm low}$ (keV)	$E_{\rm high}$ (keV)	cross section (b)	uncertainty (b)
3.994	4.482	0.958	0.020
4.482	5.028	1.281	0.021
5.028	5.642	1.097	0.016
5.642	6.331	1.004	0.014
6.331	7.103	0.912	0.013
7.103	7.970	0.919	0.013
7.970	8.942	0.848	0.013
8.942	10.033	0.817	0.012
10.033	11.257	0.800	0.012
11.257	12.631	0.787	0.012
12.631	14.172	0.761	0.012
14.172	15.902	0.729	0.011
15.902	17.842	0.685	0.011
17.842	20.019	0.613	0.010
20.019	22.461	0.641	0.010
22.461	25.202	0.566	0.009
25.202	28.277	0.545	0.009
28.277	31.728	0.513	0.008
31.728	35.599	0.497	0.009
35.599	39.943	0.468	0.009
39.943	44.816	0.456	0.008
44.816	50.285	0.413	0.007
50.285	56.421	0.365	0.006
56.421	63.305	0.346	0.006
63.305	71.029	0.318	0.006
71.029	79.696	0.275	0.005
79.696	89.421	0.248	0.005
89.421	100.332	0.229	0.005
100.332	112.574	0.220	0.004
112.574	126.310	0.204	0.004
126.310	141.722	0.192	0.004
141.722	159.016	0.172	0.003
159.016	178.418	0.179	0.003
178.418	200.188	0.165	0.003
200.188	224.614	0.158	0.003
224.614	252.022	0.159	0.003
252.022	282.773	0.156	0.002
282.773	317.277	0.147	0.002
317.277	355.990	0.144	0.002
355.990	399.428	0.141	0.002
399.428	448.165	0.140	0.002
448.165	502.849	0.158	0.002
502.849	564.207	0.154	0.002
564.207	633.051	0.164	0.001
633.051	710.294	0.178	0.001
710.294	796.963	0.179	0.001
796.963	894.207	0.156	0.001
894.207	991.452	0.135	0.001

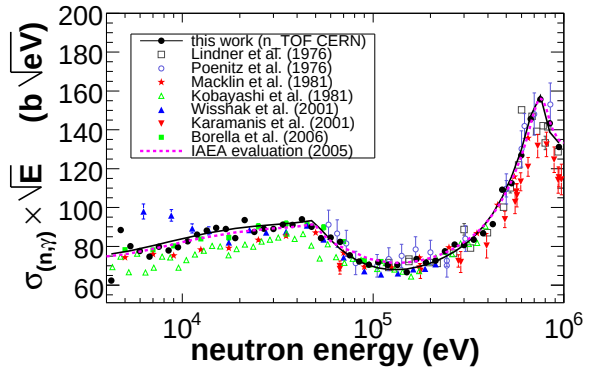

FIG. 7: (Color online) The neutron capture cross section ^{232}Th(n,γ) multiplied by the square root of the neutron energy, showing the measured data and an average parameter fit, compared to several other experimental data sets. In order to keep the figure readable, data covering energy bins are represented by points and the uncertainties for some data sets are omitted.

of the decay chain. These data show still differences with the present results ranging up to more than 10%, probably due to normalization problems. The data from these experiments are also shown in figure 7. Additional data, including resonance data, can be found elsewhere [15, 17, 20–25, 46].

We believe that many of the discrepancies with previous experiments, when exceeding the reported systematic uncertainties, could be explained from unrecognized errors on the normalization procedures, affecting the whole data set in the same way, or insufficient corrections to background estimations, applied weighting functions, or flux determinations.

In addition to these experimental data we have added in the figure a calculated cross section coming from a full evaluation of the neutron induced reactions on ^{232}Th up to 60 MeV [47] using the EMPIRE code system [48]. The calculation is based on the dispersive coupled-channel optical model potential recently developed for thorium [49] and employed a combination of the Hauser-Feshbach theory and exciton model to describe the decay of the compound nucleus. Although this calculation is not based on the measurement, the good agreement is striking. The data is also in good agreement with a recent evaluation by Maslov *et al.* [50].

C. Average parameter description of the capture cross section

The measured cross section shown in figure 7 has been fitted by an average parameter description, also shown in the figure. A different way to describe average cross sections, as a complement to optical model calculations, is to use R-matrix theory, which is usually used for resolved resonances. This procedure corresponds to a Hauser-Feshbach calculation with width fluctuations [51]. In the unresolved resonance region, fictitious resonances can be generated to describe the average cross section. These resonances enable the calculation of not only the average cross sections but also self-shielding factors in a consistent way. Therefore it is important to employ an average resonance parameter description.

The resonances in the unresolved resonance region have an average reduced neutron width $<g\Gamma_n^\ell>$ related to the neutron strength function S_ℓ by

$$S_\ell = \frac{1}{2\ell+1}\frac{<g\Gamma_n^\ell>}{D_\ell} \qquad (7)$$

where D_ℓ is the level spacing for neutron resonances of orbital momentum ℓ. In a similar way the average radiation width $<\Gamma_\gamma>$ is included. The partial cross section for a reaction from the ingoing channel c to the outgoing channel c' is then related to the average collision matrix elements $U_{cc'}$ describing the reaction by

$$<\sigma_{cc'}> = \pi\lambda\!\!\!^{-2}_c g_c <(\delta_{cc'} - U_{cc'})^2> \qquad (8)$$

The collision matrix elements $U_{cc'}$ are in their turn related to the R-matrix containing the level properties, i.e. level energies and decay amplitudes of the resonances (widths). The capture cross section can be described in this way with only a few average parameters for each partial wave.

We used the code FITACS [52] as included in SAMMY [53] to fit the average capture cross section with average resonance parameters from a Hauser-Feshbach calculation with width fluctuations. In the code the parameters that can be varied are the neutron strength functions S_ℓ, the level spacings D_ℓ, and the average radiation width $<\Gamma_\gamma>_\ell$. The energy dependence of these parameters and the competitive widths from inelastic scattering are also taken into account. The level information for the inelastic channels has been taken from the ENSDF database [54]. The contributions from the first three partial waves is sufficient up to 1 MeV.

Much care has to be taken when trying to fit these parameters from the data, since the parameters are largely correlated, in particular the parameters for a same partial wave. In addition the parameters are sensitive in a different way to the total or partial cross sections. The best way to constrain the fit to the most physical values of the parameters is to include datasets for different reaction cross sections in a simultaneous fit. In this work however we have used only the present capture data.

It may be instructive to see the contributions of each partial wave to the capture cross section as shown in figure 8. While letting free many combinations of parameters we found that is was in many cases possible to obtain a good overall fit of the capture data alone. This indicates that the parameters are strongly correlated. The plot in figure 8 has been obtained with fixed values $D_0 = 17.2$ eV for the level spacing and other parameters as given here-

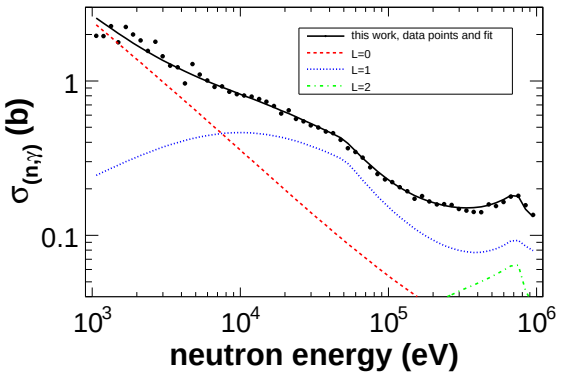

FIG. 8: (Color online) The measured cross section and a description with average resonance parameters using the code FITACS. The partial wave contribution for $\ell = 0, 1$ and 2 are also shown.

after. Variations of D_0 from 16.6 to 17.6 eV did practically not influence the following results. The values for D_1 and D_2 were scaled to D_0 by the number of allowed spin states assuming a $2J+1$ spin dependence of the level density. Values $S_0 = 0.87 \times 10^{-4}$ and $S_1 = 1.9 \times 10^{-4}$ for the neutron strength functions were taken from ref. [49]. The fitted values resulting from the code FITACS were $S_2 = 0.89 \times 10^{-4}$, $<\Gamma_\gamma>_0 = <\Gamma_\gamma>_2 = 18.8$ meV, and $<\Gamma_\gamma>_1 = 20.6$ meV. These values of the average gamma width are comparable but slightly lower than those found in the resolved resonance analysis and as found in for example [9]. We repeated the fit like before but now keeping all gamma widths fixed to $<\Gamma_\gamma>_\ell = 24.3$ meV. The resulting fitted strength functions were in that case $S_0 = 0.68 \times 10^{-4}$, $S_1 = 1.4 \times 10^{-4}$ and $S_2 = 0.43 \times 10^{-4}$.

IV. DISCUSSION OF UNCERTAINTIES

Only uncorrelated or statistical uncertainties are given in table I with the result on the measured cross section. The total uncertainty on the cross section consists of several contributions that can be identified from the analysis procedure. The main sources come from the background determination and from the absolute neutron flux determination. The uncertainty related to the influence of the weighting function is rather small in this case since the measurement is not relative to a different isotope, but it is self-normalized to the saturated resonances at 21.79 and 23.46 eV we used. The gamma-ray spectra are quite similar for the different resonances, due to the large number of levels available for decay after capture. The influence of the threshold may play a role, but the resulting cross section with a low or high threshold give statistically coherent results. From these considerations we could assign an uncertainty of 0.5% from the application of the PHWT.

The uncertainty due to background subtraction is the most delicate to estimate. The absolute level of the background requires the determination of the level of the black resonance as explained in details above. We applied several combinations of fits and binnings of the spectra and we estimate the uncertainty on the background subtraction at the level of 2.5%. This value is also in agreement with the maximum difference in cross section obtained with a threshold of 160 keV and 1000 keV.

The correction resulting from a simulation with the code SESH for self-absorption above 4 keV in at maximum about 4%. Although we had no other independent calculation to compare the correction and derive a possible uncertainty, we believe that the uncertainty on the correction is small and we have not included it in the error balance.

For the estimation of the uncertainty of the shape of the neutron flux we have adopted an uncertainty of 2%. An uncertainty on the absolute level of the flux is not relevant since we have normalized the yield on the saturated resonances.

TABLE II: The different components of the estimated systematic or correlated uncertainty on the measured cross section.

component	uncertainty (%)
PHWT	0.5
normalization	0.5
background	2.5
flux shape	2.0
total	3.3

Adding up these components gives a total correlated or systematical uncertainty of 3.5% listed in the table II. A detailed covariance propagation for the present analysis procedure and within the given assumptions on the uncertainty contributions is described in a separate report [55].

V. CONCLUSION

A new set of self-normalized ^{232}Th neutron capture yield data has been obtained in a large energy range from 1 eV to 1 MeV from a measurement at n_TOF at CERN. The cross section in the unresolved resonance region from 4 keV to 1 MeV has been extracted and the results have been fitted in terms of average resonance parameters. The point-wise data have been reported in logarithmically equidistant energy bins with 20 bins per energy decade. A comparison with existing data has solved an important discrepancy in the 10 keV region and increased the present knowledge of the capture cross section up to 1 MeV.

The present measurement covers a large energy range including the both the endpoints of other time-of-flight measurements and the starting energies of activation measurements.

Without giving into details going beyond the scope of this paper, it is clear that the accurate knowledge of this cross section is of great importance for a thorium-based nuclear fuel cycle. In addition, the precisely measured cross section puts severe constraints on optical model calculations predicting cross sections for this nucleus. Additional information is expected from the analysis of the resolved resonances below 4 keV.

Acknowledgments

This work has been supported by the European Commission's 5th Framework Programme under contract number FIKW-CT-2000-00107 (n_TOF-ND-ADS Project).

[1] G. Wallerstein et al., Rev. Mod. Phys. **69**, 995 (1997).
[2] F. Käppeler, Progress in Particle and Nuclear Physics **43**, 419 (1999).
[3] G. E. Mitchell, J. D. Bowman, and H. A. Weidenmüller, Rev. Mod. Phys. **71**, 445 (1999).
[4] Y. Masuda et al., Nucl. Phys. A **721**, 485C (2003).
[5] M. Salvatores, I. Slessarev, and A. Tchistiakov, Nucl. Sci. Eng. **130**, 309 (1998).
[6] W. Gudowski, Nucl. Phys. A **654**, 436c (1999).
[7] S. David, A. Billebaud, M. E. Brandan, R. Brissot, A. Giorni, D. Heuer, J. M. Loiseaux, O. Meplan, H. Nifenecker, J. B. Viano, et al., Nucl. Instrum. Methods Phys. Res. Sect. A **443**, 510 (2000).
[8] A. Bidaud, Ph.D. thesis, University Paris XI, Orsay (2005).
[9] S. F. Mughabghab, M. Divadeenam, and N. E. Holden, *Neutron cross sections: Neutron resonance parameters and thermal cross sections. Z=1-60* (Academic Press, 1981).
[10] S. I. Sukhoruchkin, Z. N. Soroko, and V. V. Deriglazov, *Low Energy Neutron Physics, Volume I/16B, Tables of Neutron Resonance Parameters* (Springer, Landolt-Börnstein, 1998).
[11] See for example the International Atomic Energy Agency (IAEA) on www-nds.iaea.org, or the OECD Nuclear Energy Agency on www.nea.fr.
[12] G. E. Mitchell, J. D. Bowman, S. I. Pentillä, and E. I. Sharapov, Phys. Rep. p. 157 (2001).
[13] S. L. Stephenson et al., Phys. Rev. C **58**, 1236 (1998).
[14] J. D. Bowman, G. T. Garvey, M. B. Johnson, , and G. E. Mitchell, Annu. Rev. Nucl. Part. Sci. **43**, 829 (1993).
[15] F. Rahn et al., Phys. Rev. C **6**, 1854 (1972).
[16] M. Lindner, R. J. Nagle, and J. H. Landrum, Nucl. Sci. Eng. **59**, 381 (1976).
[17] R. L. Macklin and J. Halperin, Nucl. Sci. Eng. **64**, 849 (1977).
[18] W. P. Poenitz and D. L. Smith, Nucl. Sci. Eng. **59**, 381 (1976).
[19] K. Kobayashi, Y. Fujita, and N. Yamamuro, J. Nucl. Sci. Techn. p. 823 (1981).
[20] R. L. Macklin, Nucl. Sci. Eng. **79**, 118 (1981).
[21] D. K. Olsen, R. W. Ingle, and J. L. Portney, Nucl. Sci. Eng. **82**, 289 (1982).
[22] R. B. Perez, G. de Saussure, R. L. Macklin, J. Halperin, and N. W. Hill, Nucl. Sci. Eng. **80**, 189 (1982).
[23] K. Kobayashi et al., Ann. Nucl. Energy **15**, 381 (1988).
[24] W. Y. Baek, G. N. Kim, M. H. Cho, I. S. Ko, W. Namkung, Y. V. Grigoriev, H. Faikov-Stanczyk, V. N. Shvetshov, and W. I. Furman, Nucl. Instrum. Methods Phys. Res. Sect. B **168**, 453 (2000).
[25] Y. V. Grigoriev et al., J. Nucl. Sci. and Tech. **supp. 2**, 350 (2002).
[26] A. Borella, K. Volev, A. Brusegan, G. Lobo, P. Schillebeeckx, F. Corvi, N. Koyumdjieva, N. Janeva, and A. A. Lukyanov, Nucl. Sci. Eng. **152**, 1 (2006).
[27] K. Wisshak, F. Voss, and F. Käppeler, Nucl. Sci. Eng. **137**, 183 (2001).
[28] D. Karamanis et al., Nucl. Sci. Eng. **139**, 282 (2001).
[29] G. Aerts et al., in preparation (2006).
[30] G. Aerts, Ph.D. thesis, University Paris XI, Orsay (2005).
[31] C. Rubbia et al., Tech. Rep. CERN/LHC/98-02, CERN (1998).
[32] U. Abbondanno et al., Tech. Rep. CERN-SL-2002-053 ECT (2003).
[33] J. Pancin et al., Nucl. Instrum. Methods Phys. Res. Sect. A **524**, 102 (2004).
[34] U. Abbondanno et al., Tech. Rep. CERN/INTC 2001-038 (2001).
[35] A. Ferrari, C. Rubbia, and V. Vlachoudis, Tech. Rep. CERN-SL-EET-2001-036, CERN (2002).
[36] R. Plag et al., Nucl. Instrum. Methods Phys. Res. Sect. A **496**, 425 (2003).
[37] S. Marrone et al., Nucl. Instrum. Methods Phys. Res. Sect. A **517**, 389 (2004).
[38] C. Borcea et al., Nucl. Instrum. Methods Phys. Res. Sect. A **513**, 524 (2003).
[39] U. Abbondanno et al., Nucl. Instrum. Methods Phys. Res. Sect. A **538**, 692 (2005).
[40] F. Bečvář, Nucl. Instrum. Methods Phys. Res. Sect. A **417**, 434 (1998).
[41] F. Corvi et al., Nucl. Sci. Eng. **107**, 272 (1991).
[42] J. N. Wilson, B. Haas, S. Boyer, D. Dassié, G. Barreau, M. Aiche, S. Czajkowski, C. Grosjean, and A. Guiral, Nucl. Instrum. Methods Phys. Res. Sect. A **511**, 388 (2003).
[43] U. Abbondanno et al., Nucl. Instrum. Methods Phys. Res. Sect. A **521**, 454 (2004).
[44] F. H. Fröhner, SESH, computer code GA-8380, Gulf General Atomic (1968).
[45] R. L. Macklin and R. R. Winters, Nucl. Sci. Eng. **78**, 110 (1981).
[46] G. Baldwin and G. Knoll, Nucl. Sci. Eng. **88**, 121 (1984).
[47] R. Capote, M. Sin, and A.Trkov, **in preparation** (2005).
[48] M. Herman et al., *Nuclear reaction model code EMPIRE v.2.19*, URL `www-nds.iaea.org/empire/`.
[49] E. S. Soukhovitskii, R. Capote, J. M. Quesada, and S. Chiba, Phys. Rev. C **72**, 024604 (2005).
[50] V. M. Maslov et al., Tech. Rep. Report INDC(BLR)-016, International Atomic Energy Agency (2003).
[51] F. H. Fröhner, Nucl. Sci. Eng. **103**, 119 (1989).
[52] F. H. Fröhner, B. Goel, and U. Fischer, FITACS, computer code Report ANL-83-4, Argonne National Labora-

tory (1983).
[53] N. M. Larson, SAMMY, computer code Report ORNL/TM-9179/R7, Oak Ridge National Laboratory (2006).
[54] See for example www.nndc.bnl.gov.
[55] H. Leeb and M. Pigni, Tech. Rep. Report ATI-NDC-2004-03, Technische Universität Wien (2005).